Supporting Information

Enhanced Separation Performance forCO_2 gas of Mixed-Matrix Membranes Incorporated of TiO_2/Graphene Oxide: Synergistic Effect of Graphene Oxide and Small TiO_2 Particles on Gas Permeability of Membranes

*Ting Wang[a], Cai-hong Yang[a], Chun-Li Man[a], Li-guang Wu[a, *], Wan-lei Xue[a], Jiang-nan Shen[b], Bart Van der Bruggen[c], ZhuanYi[a]*

[a] School of Environ. Sci. & Eng., Zhejiang Gongshang University, Hangzhou, 310012, China

[b] Center for Membrane and Water Science, Ocean College, Zhejiang University of Technology, Hangzhou 310014, China

[c] Department of Chemical Engineering, Process Engineering for Sustainable Systems (ProcESS), KU Leuven, Celestijnenlaan 200F, B-3001 Leuven, Belgium

Preparation of graphene oxide with hydrophilic groups

GO nanosheets with hydrophilic groups were synthesized through the oxidization of graphite powder based on the previously reported improved Hummers method followed by ultrasonication[1]. Previous results showed that GO nanosheets induced an optimized morphology and distribution in polymer matrices when 5.0 g graphite powder, 2.5g of $NaNO_3$, and 20 g of $KMnO_4$ were added to the suspension during GO preparation. Therefore, these conditions, considered as optimized, were maintained in the present study for the synthesis of GO nanosheets.

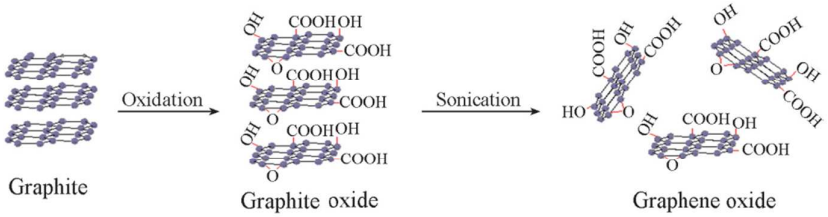

Scheme S1The formation mechanism of GO nanosheets by improved Hummers method

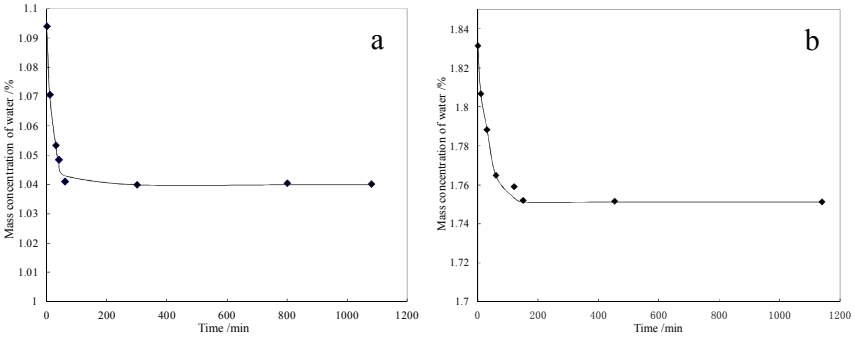

Figure S1 Dependences of water adsorbed by GO on adsorption time

a. 1.5 mL of water; b. 3.0 mL of water

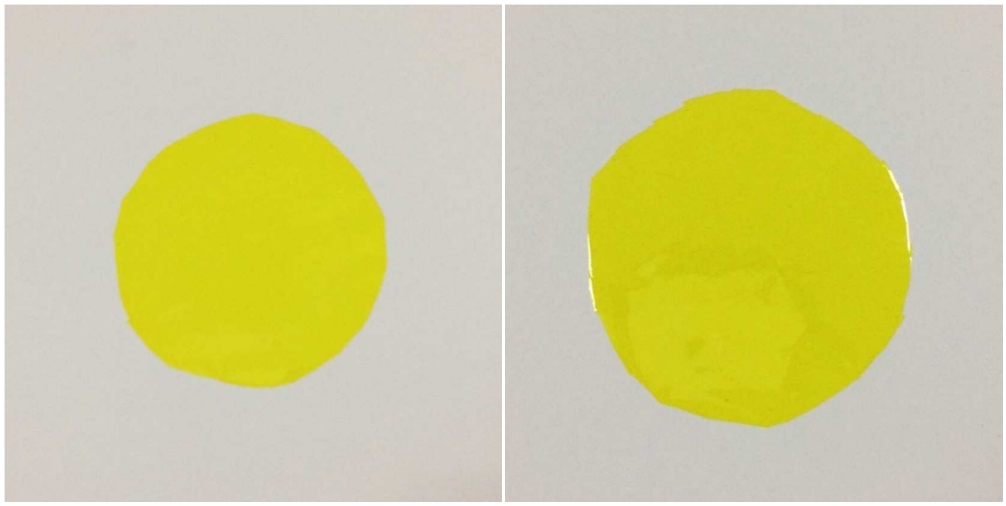

Figure S2 Digital photos of PI polymer membrane with or without heating at 350 ^{o}C for 1 h

From the figures, it is found that the morphology of PI polymer membrane change little after heating at 350 ^{o}C for 1 h, due to the high thermal stability of PI polymer.

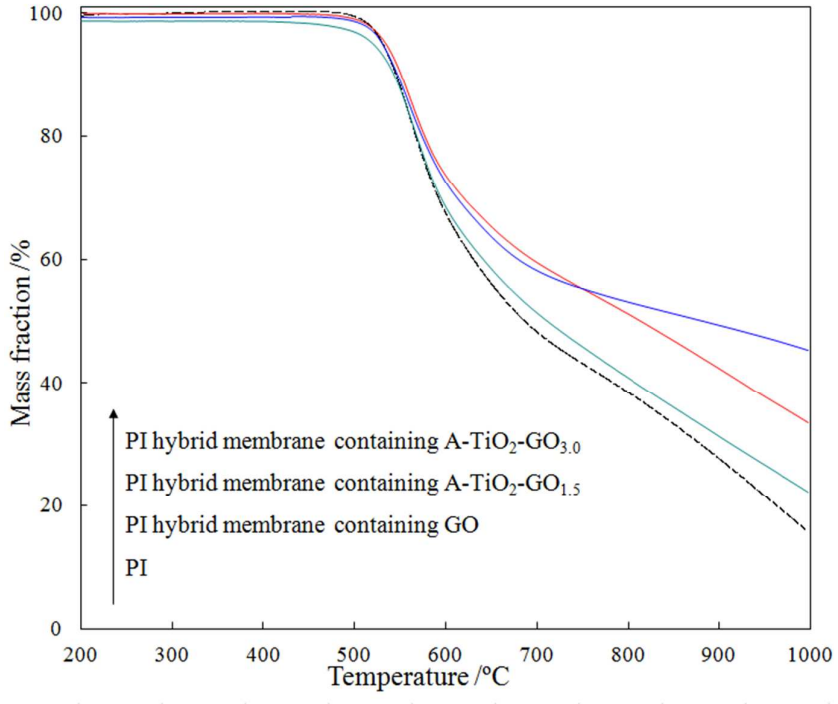

Figure S3 TGA thermograms of PI and different PI hybrid membranes

From the figure, the PI and PI hybrid membranes all show the similar high thermal stability, due to the high thermal stability of PI polymer. When temperature was less than 500 °C, there no

quality loss observed in the TGA thermograms. This also confirmed that GO nanosheets and TiO_2 particles would be protected well in PI polymer matrix, during the polymerization process. It is also found in TGA thermograms that addition of GO or A-TiO_2-GO samples will improve a little the thermal stability of membranes.

Gas permeability measurements

The pure gas permeability values were determined using the constant-volume/variable-pressure method [2, 3], in which a specimen was held under vacuum at 30 °C until it was exposed to a gas at a specific pressure. The increase in permeation pressure as a function of time was measured using a pressure transducer. The permeabilities of all gases were measured at 30 °C and a constant pressure of 10 bar. In order to avoid the interference of CO_2, the gas permeability measurement with pure N_2 was first carried out for all membranes in this work. The gas permeability was determined using Eq. (1):

$$P = D \times S = 10^{10} \times \frac{VL}{p_{up}ART} \times \frac{dp(t)}{dt}, \quad (1)$$

where P is the gas permeability in Barrer [1Barrer=10^{-10} cm^3 (STP) cm cm^{-2} s^{-1} cm Hg^{-1}], p_{up} is the upstream pressure (cm Hg), dp/dt is the steady-state permeate-side pressure increase (cm Hgs^{-1}), V is the calibrated permeate volume (cm^3), L is the membrane thickness (cm), A is the effective membrane area (cm^2), T is the operating temperature (K), and R is the gas constant [0.278 cm^3 cm Hg cm^{-3}(STP)K^{-1}].

The diffusivity (D) was determined according to Eq. (2):

$$D = {L^2}/{6\theta}, \quad (2)$$

where θ is the time lag when a steady dp/dt rate is obtained on the downstream side of the permeation tests [4]. The solubility (S) was estimated by means of Eq. (3):

$$S = {P}/{D}, \quad (3)$$

and the ideal selectivity (α) was determined using Eq. (4):

$$\alpha = {}^{P_A}/_{P_B} = {}^{D_A}/_{D_B} \cdot {}^{S_A}/_{S_B} = \alpha_D \cdot \alpha_S. \quad (4)$$

Here, P_A and P_B are the permeabilities of pure gases CO_2 and N_2, respectively. The terms α_D and α_S are the solubility selectivity and diffusivity selectivity, respectively. The solution–diffusion transport model [5]was used to discuss the gas transport properties of dense hybrid membranes containing different TiO_2-GO samples.

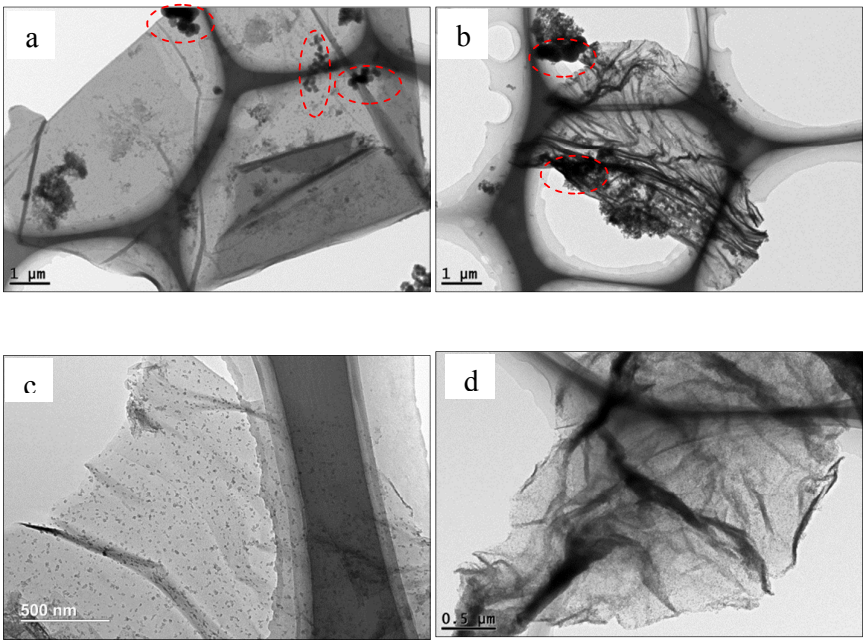

Figure S4 TEM images with wide range of different TiO_2-GO samples

a. P-TiO_2-$GO_{1.5}$; b. P-TiO_2-$GO_{3.0}$; c. A-TiO_2-$GO_{1.5}$; d. A-TiO_2-$GO_{3.0}$.

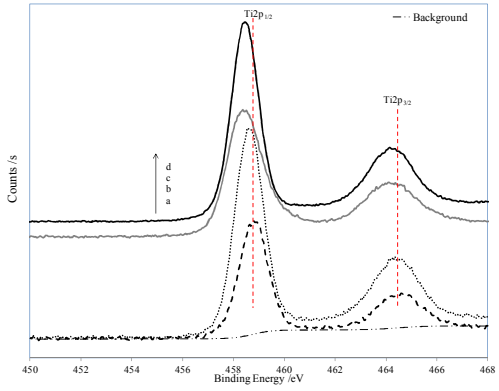

Figure S5 XPS profiles of Ti2p in differentTiO_2-GO samples

a. P-TiO_2-$GO_{1.5}$; b. P-TiO_2-$GO_{3.0}$; c. A-TiO_2-$GO_{1.5}$; d. A-TiO_2-$GO_{3.0}$.

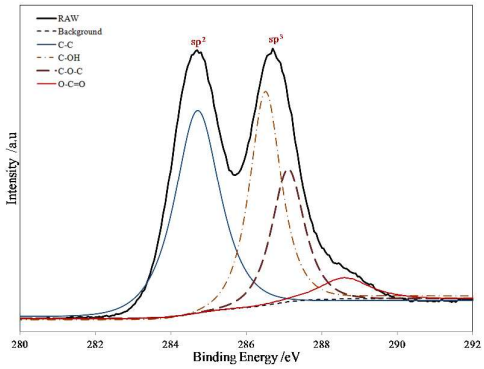

Figure S6 XPS profiles of C1s in GO samples

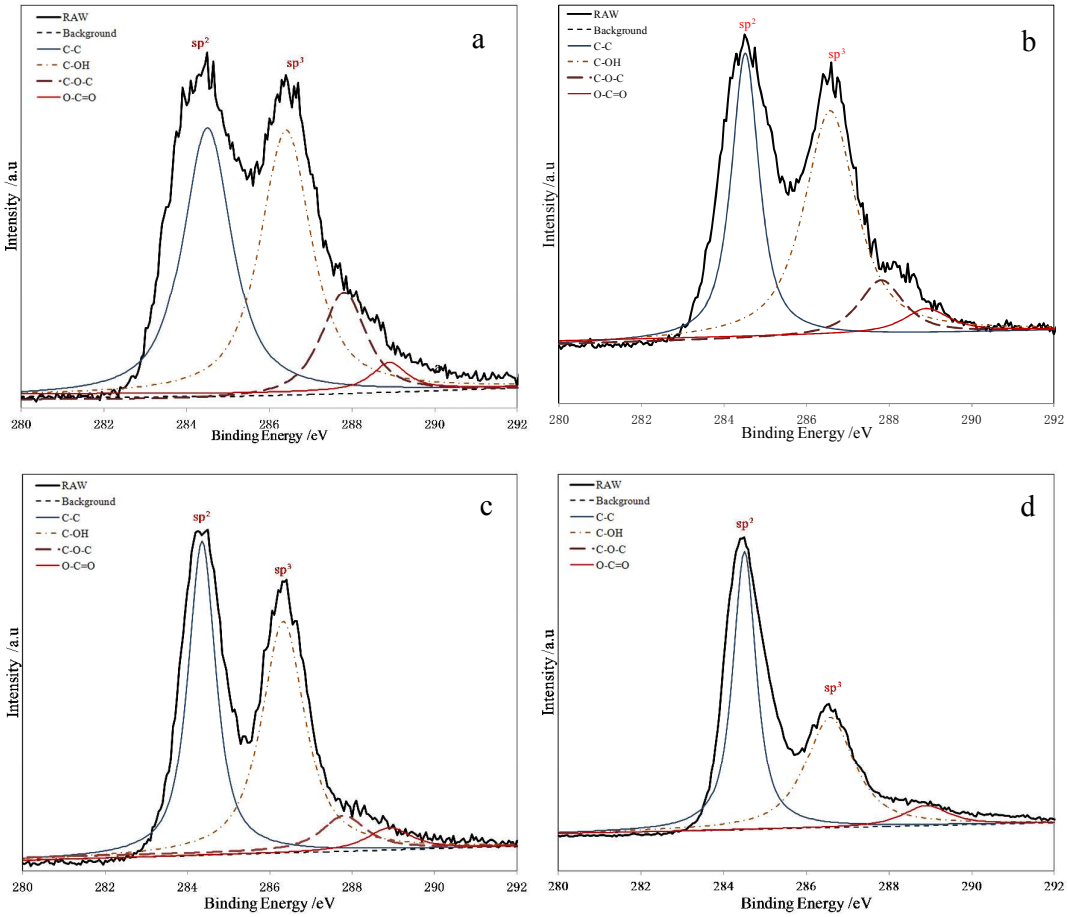

Figure S7 XPS profiles of C1s in different TiO_2-GO samples

a. P-TiO_2-$GO_{1.5}$; b. P-TiO_2-$GO_{3.0}$;c. A-TiO_2-$GO_{1.5}$;d. A-TiO_2-$GO_{3.0}$.

The peak at 284.5 eVis assigned to the sp^2-hybridized carbon atoms [6] and the other peak originates from C-O of the GO or TiO_2-GOsurface samples with sp^3-hybridized orbitals.

Moreover, the intensity of the sp^2-hybridized C1s peak in TiO_2-GO samples, particularly both A-TiO_2-GO samples, becomes stronger compared to that of the GO sample.

FIIR spectra

Figure S8 suggests that the characteristic FTIR profile of TiO_2–GO samples is similar to that of the GO sample. The main absorption bands are found at 1620 cm^{-1} (C–C stretching), 1392cm^{-1} (C-OH stretching), and 1042 cm^{-1}(C-O stretching) [7]. The peak at 3383 cm^{-1} consists of a resonance peak assigns to absorbed hydroxyl groups in the samples [8].

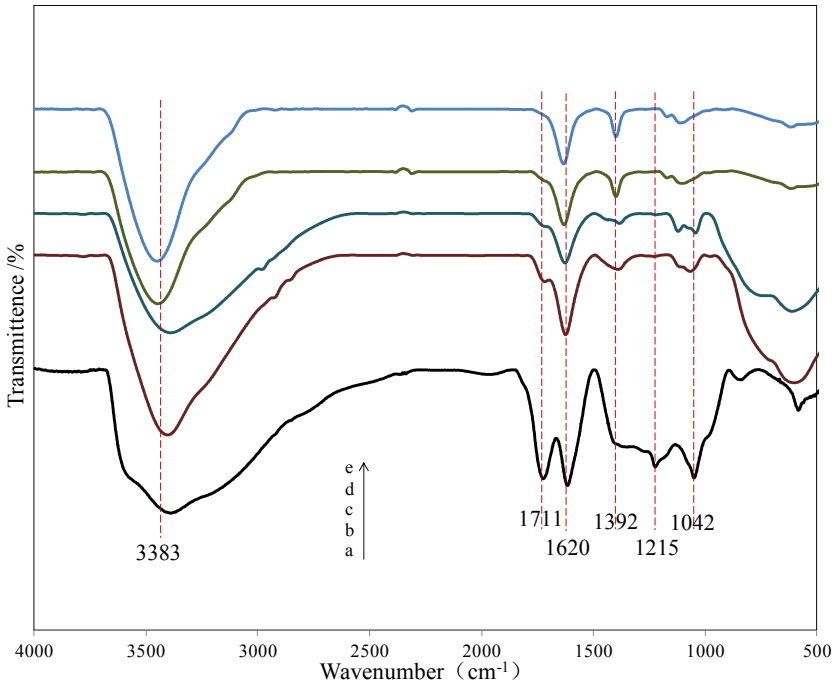

Figure S8 FTIR spectra of GO and different TiO_2-GO samples.

a. GO; b. P-TiO_2-$GO_{1.5}$; c. P-TiO_2-$GO_{3.0}$; d. A-TiO_2-$GO_{1.5}$; e. A-TiO_2-$GO_{3.0}$

Raman spectra

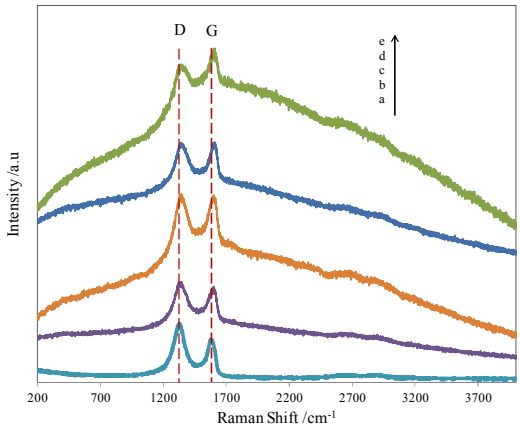

Figure S9 Raman spectra of GO and different TiO_2-GO samples.

(excitation at λ = 632.8 nm)

a. GO; b. P-TiO_2-$GO_{1.5}$; c. P-TiO_2-$GO_{3.0}$; d. A-TiO_2-$GO_{1.5}$; e. A-TiO_2-$GO_{3.0}$

The Raman spectra show two obvious characteristic peaks for GO and the four TiO_2-GO samples. The first peak at approximately 1350 cm^{-1} was linked to the disordered carbon band (D-band) and typically assigned to surface defects on GO sheets. The second peak at about 1580 cm^{-1} represents the graphitized band (G-band), which corresponds to the formation of sp^2-bonded crystalline carbon in GO samples [9, 10].

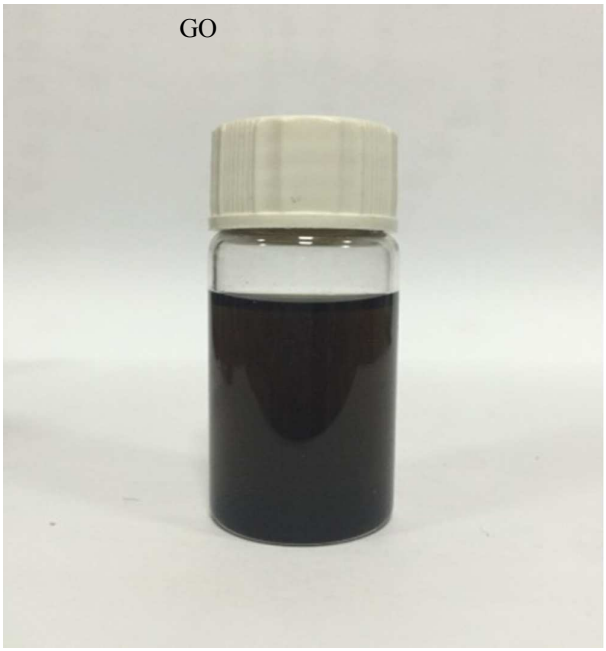

Figure S10 Digital photos of GO in DMAC after 24 h

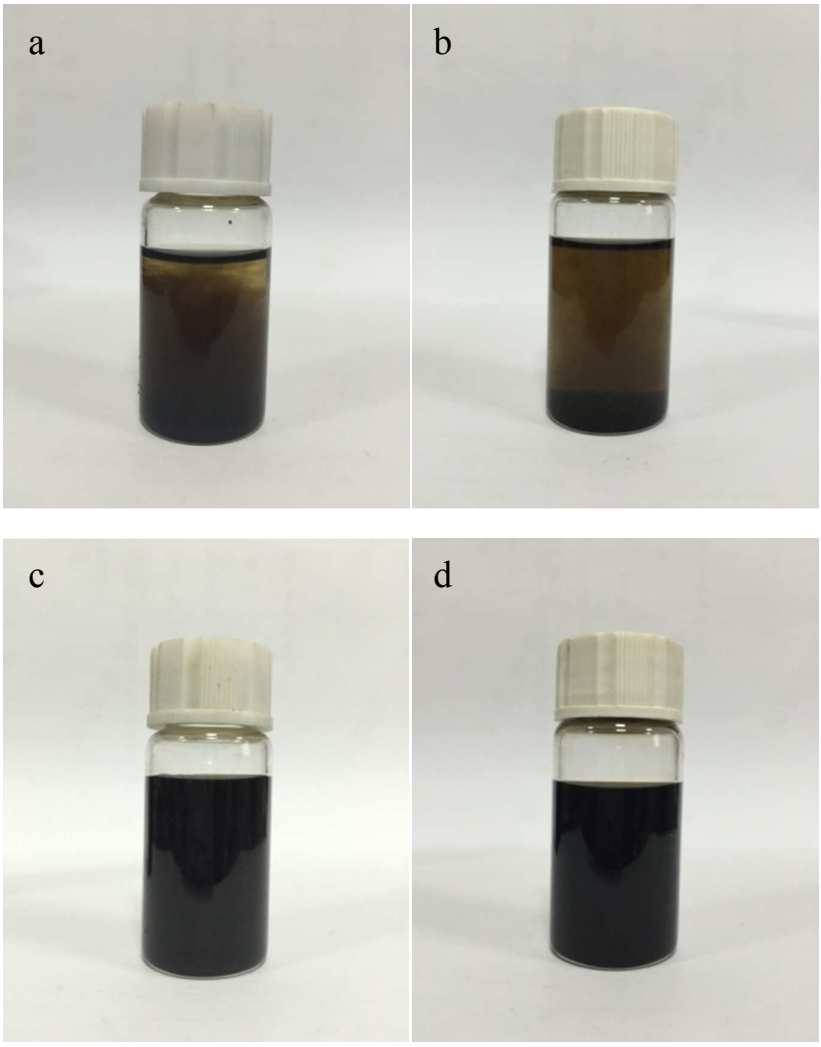

Figure S11 Digital photos of different TiO_2-GO samples in DMAC after 24 h

a. P-TiO_2-$GO_{1.5}$; b. P-TiO_2-$GO_{3.0}$;c. A-TiO_2-$GO_{1.5}$;d. A-TiO_2-$GO_{3.0}$.

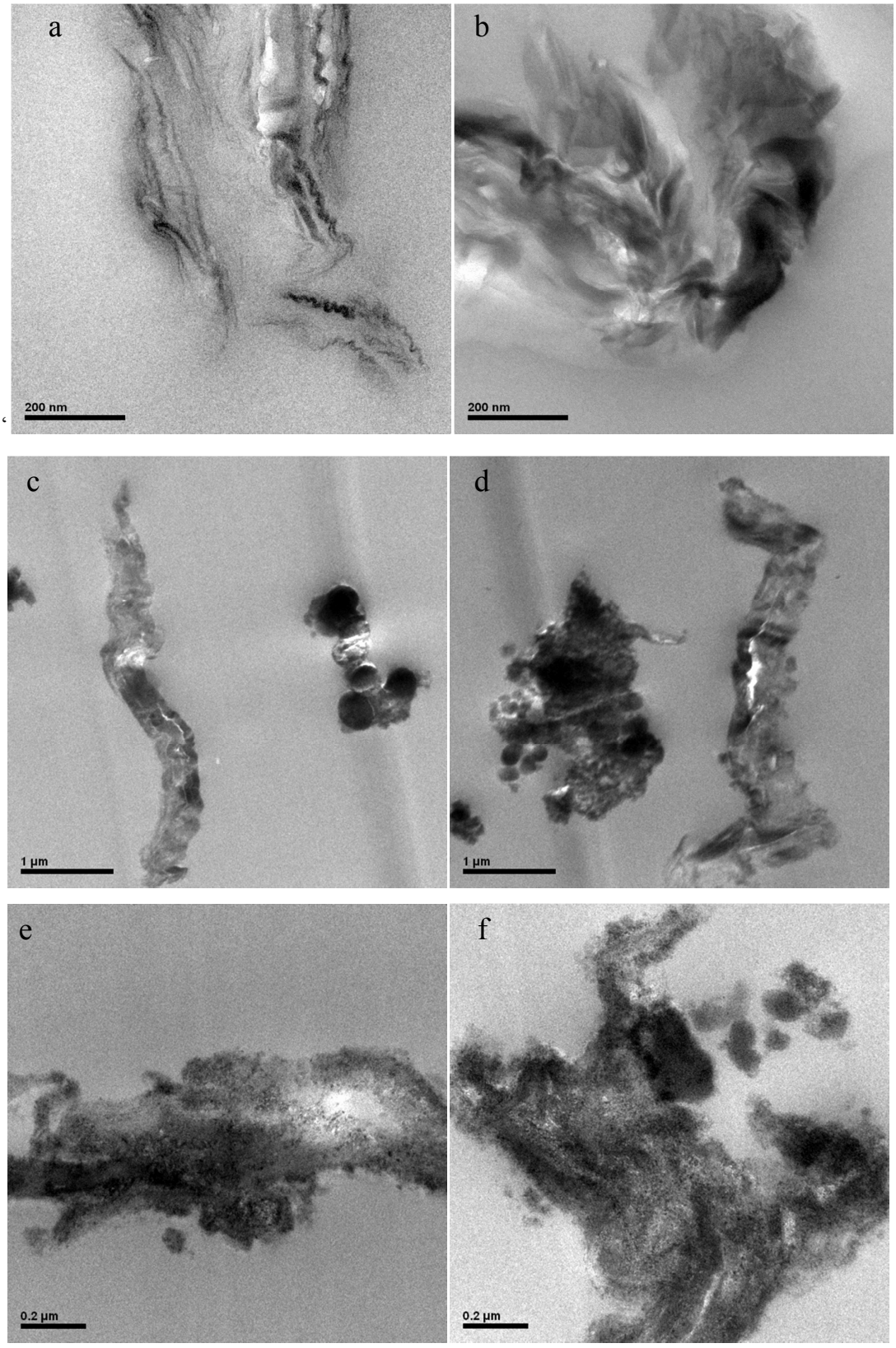

Figure S12 TEM images of hybrid membranes containing different TiO_2-GO samples

a. GO-PU membrane; b. GO-PI membrane;

c. P-TiO_2-GO/PU; d. P-TiO_2-GO/PI; e. A-TiO_2-GO/PU; f. A-TiO_2-GO/PI

(3.0 mL of water in preparation of TiO_2-GO samples)

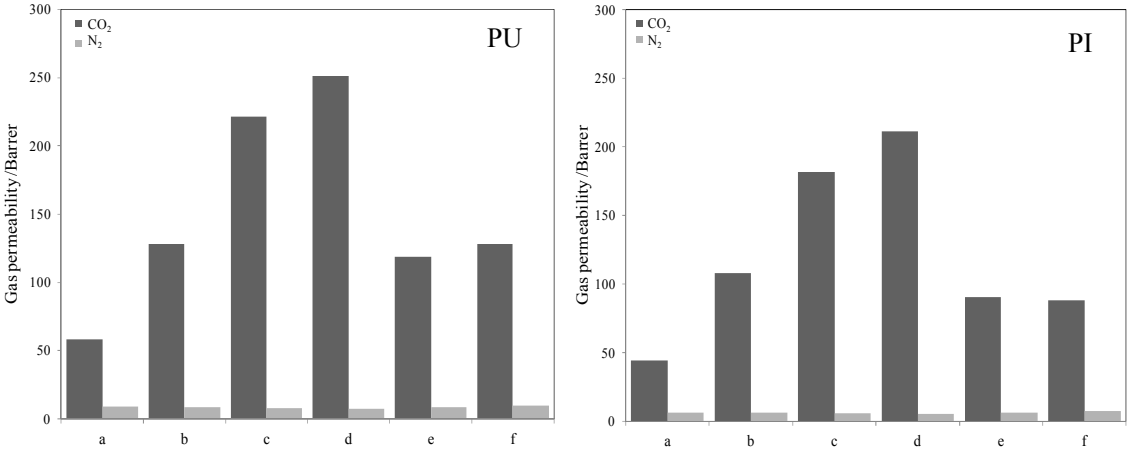

Figure S13 The gas permeability of PU or PI and different hybrid membranes.

a. PU or PI membranes; b. Membranes with GO; c. Membranes with A-TiO_2-$GO_{1.5}$;

d. Membranes with A-TiO_2-$GO_{3.0}$; e. Membranes with P-TiO_2-$GO_{1.5}$; f. Membranes with

P-TiO_2-$GO_{3.0}$

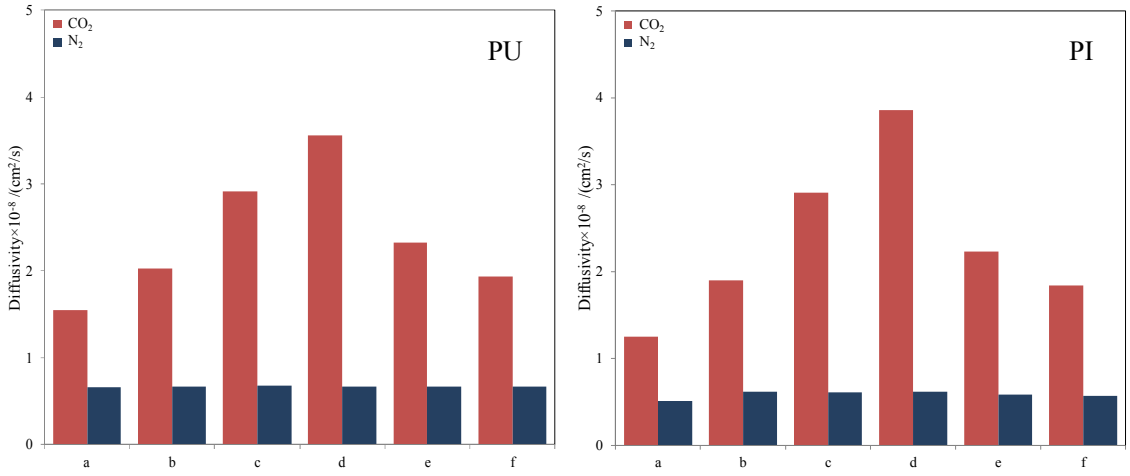

Figure S14 The diffusivity through PU or PI and different hybrid membranes.

a. PU or PI membranes; b. Membranes with GO; c. Membranes with A-TiO_2-$GO_{1.5}$;

d. Membranes with A-TiO_2-$GO_{3.0}$; e. Membranes with P-TiO_2-$GO_{1.5}$; f. Membranes with

P-TiO_2-$GO_{3.0}$.

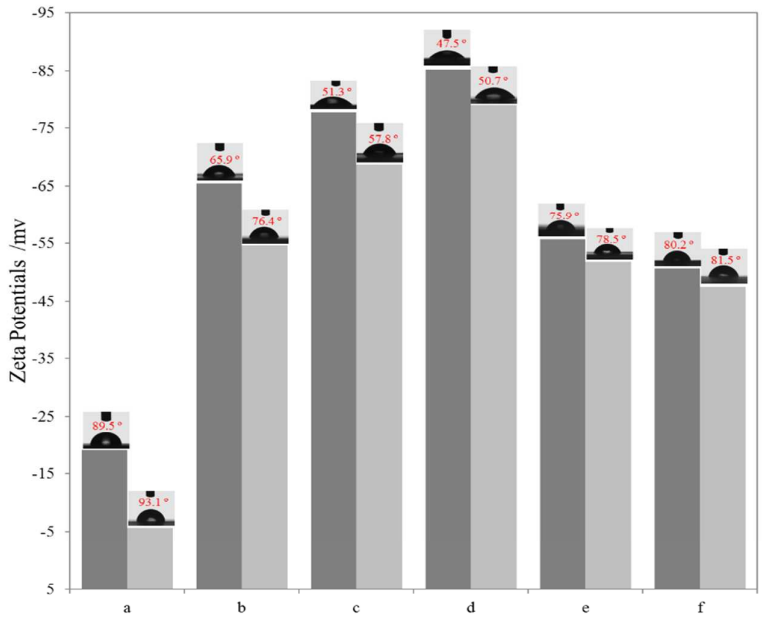

Figure S15 Zeta potential values and water contact angles of different hybrid membranes.

a. PU or PI membranes; b. Membranes with GO;

c. Membranes with A-TiO_2-$GO_{1.5}$; d. Membranes with A-TiO_2-$GO_{3.0}$;

e. Membranes with P-TiO_2-$GO_{1.5}$; f. Membranes with P-TiO_2-$GO_{3.0}$.

The zeta potential values and water contact angles are used to characterize the surface electrical properties of mixed matrix membranes [1]. The parameters are closely related to the content and dispersion of GO or TiO_2-GO. GO or TiO_2-GO with polar functional groups tend to disperse homogeneously in the mixed matrix membranes, which leads to larger zeta potential values and smaller water contact angles for the mixed matrix membrane. The hybrid membranes containing A-TiO_2-$GO_{3.0}$ samples have the largest zeta potential value and the smallest water contact angles, due to the presence of the most well-distributed small TiO_2 particles on GO nanosheets.

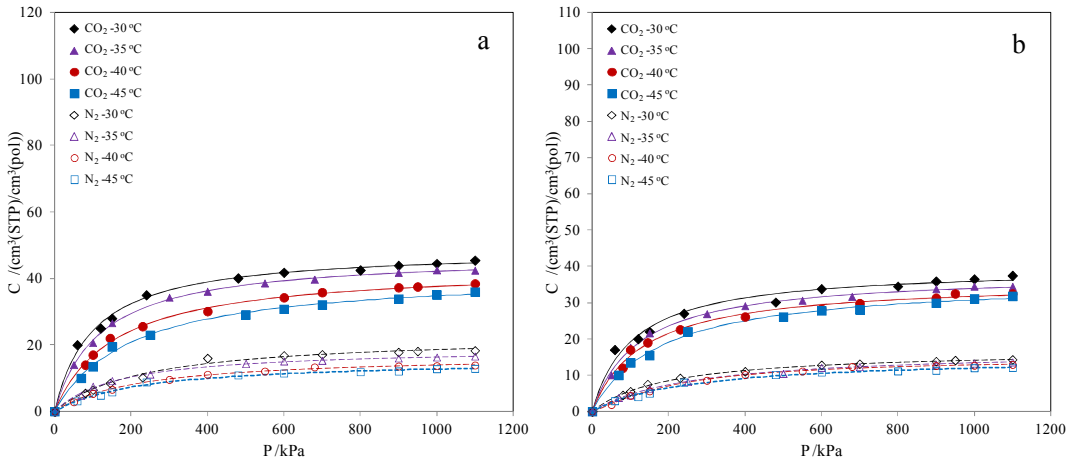

Figure S16 CO_2 and N_2 sorption isotherms of PU and PI membranes at 30 ℃, 35 ℃, 40 ℃, and 45 ℃

a. PU; b. PI

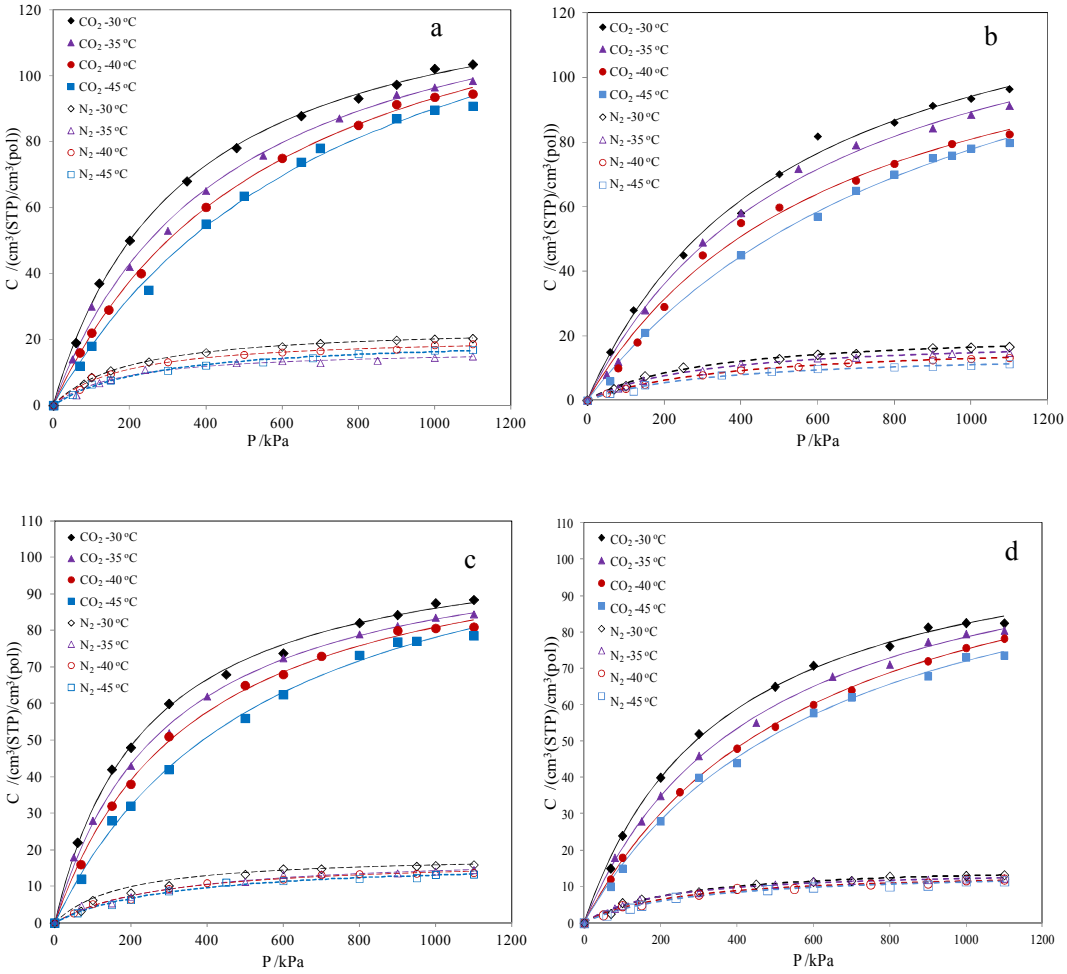

Figure S17 CO_2 and N_2 sorption isotherms of different hybrid membranes at 30 °C, 35 °C, 40 °C, and 45 °C

a. PU membranes with P-TiO_2-$GO_{1.5}$; b. PU membranes with P-TiO_2-$GO_{3.0}$;

c. PI membranes with P-TiO_2-$GO_{1.5}$; d. PI membranes with P-TiO_2-$GO_{3.0}$.

(The GO content in all hybrid membranes was 1.0 wt%)

The TPD-CO_2 results were used to investigate the adsorption and affinity between the prepared samples and CO_2 gas molecules. Figure S14 shows strong intensity peaks ranging from 200 to 350 °C in the CO_2 desorption curves of GO and TiO_2-GO samples, suggesting that all samples strongly absorbed CO_2 and thus a strong affinity exists between CO_2 and GO or TiO_2-GO samples. Therefore, the addition of GO and TiO_2-GO samples all cause a high solubility selectivity in the hybrid membrane, but the solubility selectivity of the two types of hybrid membranes was similar under the same conditions. The P-TiO_2-GO shows similar desorption curves as GO, indicating that the large TiO_2particles in P-TiO_2-GO slightly changes the adsorption of CO_2 gas. This confirms that the decrease insolubility selectivity of the hybrid membranes with incorporation of two P-TiO_2-GO is caused by aggregations in the membranes.

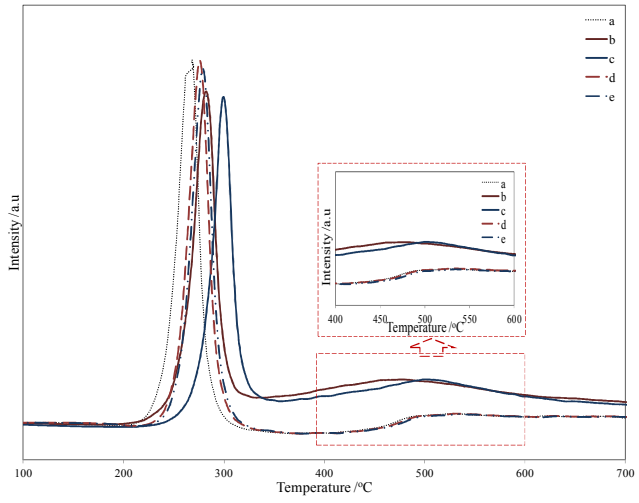

Figure S18 CO_2-TPD results of GO and different TiO_2-GO samples.

a. GO; b. A-TiO_2-$GO_{1.5}$; c. A-TiO_2-$GO_{3.0}$; d. P-TiO_2-$GO_{1.5}$; e. P-TiO_2-$GO_{3.0}$

For both A-TiO_2-GO samples, a wide but weak desorption peak ranging from 350 to 600 °C was present in both the desorption curves. This could be caused by a combination of TiO_2 small particles and CO_2 molecules. Except this, the strong desorption peak displayed between 200 to

350 °C of A-TiO_2-GO samples shifted to higher temperatures compared to that of GO and P-TiO_2-GO samples. This demonstrates the strong affinity between A-TiO_2-GO samples and CO_2 molecules, indicating that the small TiO_2particles would slightly increase the solution selectivity of the hybrid membranes. Thus, the hybrid membranes incorporated by A-TiO_2-GO resulted in a slightly higher solution selectivity.

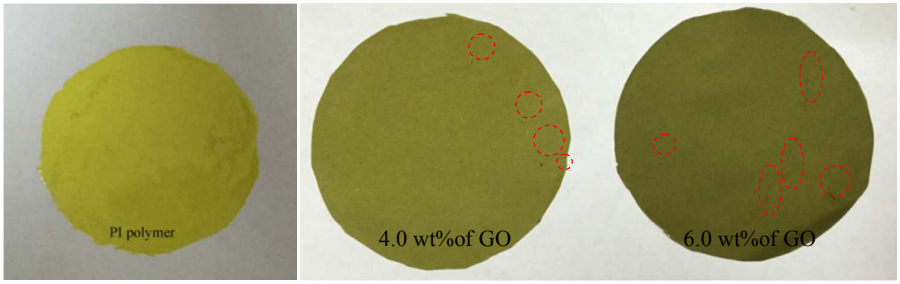

Figure S19 Photographs of PI membrane and GO/PI hybrid membranes

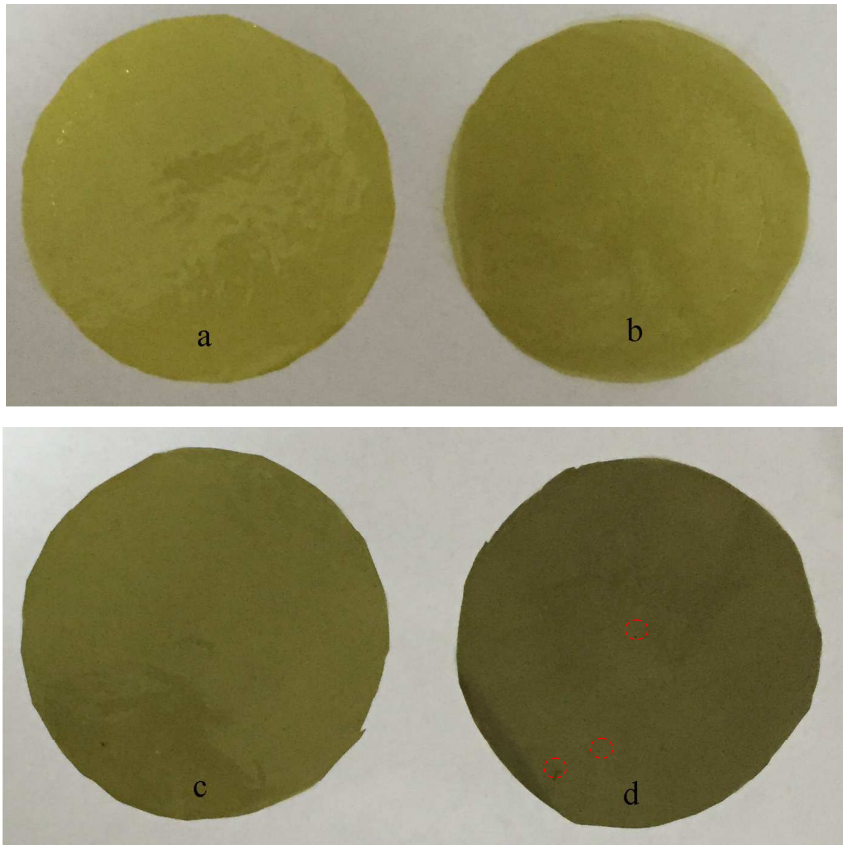

Figure S20 Photographs of PI hybrid membranes containing different A-TiO_2-GO samples a. A-TiO_2-$GO_{1.5}$ and 4 wt% GO in hybrid membranes; b. A-TiO_2-$GO_{3.0}$ and 4 wt% GO in hybrid membranes; c. A-TiO_2-$GO_{1.5}$ and 6 wt% GO in hybrid membranes;

d. A-TiO_2-$GO_{3.0}$ and 6 wt% GO in hybrid membranes.

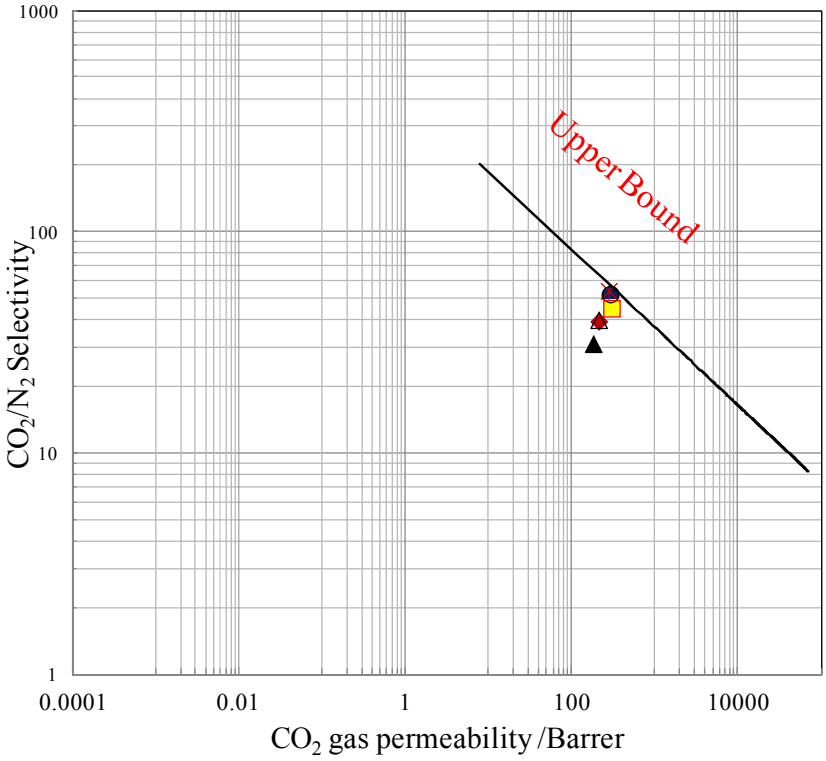

Figure S21 CO_2/N_2 Ideal selectivities of different PI hybrid membranes

▲ A-TiO_2-$GO_{1.5}$/PI (1.0 wt% loading of GO); ◆ A-TiO_2-$GO_{1.5}$/PI (2.0 wt% loading of GO);

● A-TiO_2-$GO_{1.5}$/PI (4.0 wt% loading of GO); ■ A-TiO_2-$GO_{1.5}$/PI (6.0 wt% loading of GO);

△ A-TiO_2-$GO_{3.0}$/PI (1.0 wt% loading of GO); X A-TiO_2-$GO_{3.0}$/PI (2.0 wt% loading of GO);

○ A-TiO_2-$GO_{3.0}$/PI (4.0 wt% loading of GO); □ A-TiO_2-$GO_{3.0}$/PI (6.0 wt% loading of GO)

Table S1 The C/O atomic ratio in GO and different TiO_2-GO samples

Sample	GO	P-TiO_2-$GO_{1.5}$	P-TiO_2-$GO_{3.0}$	A-TiO_2-$GO_{1.5}$	A-TiO_2-$GO_{3.0}$
C/O atomic ratio	2.13	3.68	3.45	4.21	4.02

Table S2 Separation performance of different hybrid membranes using a mixture of CO_2/N_2 (1:9 v/v) as test gas

Sample	GO content /%	Gas permeability /Barrer		Selectivities (α_{CO_2/N_2})
		CO_2	N_2	
A-TiO_2-$GO_{1.5}$/PI	1	177.35	5.62	31.56
	2	220.77	5.77	38.26
	4	281.12	5.43	51.77
	6	291.11	6.41	45.41
A-TiO_2-$GO_{3.0}$/PI	1	214.89	5.48	39.21
	2	289.99	5.59	51.88
	4	297.32	5.74	51.80
	6	310.25	6.71	46.24

REFERENCES

(1) Wang, T.; Zhao, L.; Shen, J. N.; Wu, L. G.; Bruggen, B. V. Enhanced Performance of Polyurethane Hybrid Membranes for CO_2Separation by Incorporating Graphene Oxide: The

Relationship between Membrane Performance and Morphology of Graphene Oxide. *Environ. Sci. Technol.* **2015**, *49*, 8004−8011.

(2) Cong, H. L.; Yu, B. Aminosilane Cross-Linked PEG/PEPEG/PPEPG Membranes for CO_2/N_2 and CO_2/H_2Separation. *Ind. Eng. Chem. Res.* **2010**, *49*, 9363−9369.

(3) Yu, B.; Cong, H. L.; Zhao, X. S. Hybrid Brominated Sulfonated Poly(2,6-diphenyl-1,4-phenyleneoxide) and SiO_2 Nanocomposite Membranes for CO_2/N_2 Separation. *Prog. Nat. Sci.* **2012**, *22*, 661−667.

(4) Car, A.; Stropnik, C.; Yave, W.; Peinemann, K. V. PEG Modified Poly(amide-b-ethylene oxide) Membranes for CO_2 Separation. *J. Membr. Sci.* **2008**, *307*, 88−95.

(5) Wijmans, J. G.; Baker, R. W. The Solution–Diffusion Model: A Review. *J. Membr. Sci.* **1995**, *107*, 1−21.

(6)Lee, D. W.; Seo, J.W. Sp^2/sp^3 Carbon Ratio in Graphite Oxide with Different Preparation Times. *J. Phys. Chem. C* **2011**, *115*, 2705–2708.

(7)Xu, C.; Wang, X. ; Zhu, J. W. Graphene–Metal Particle Nanocomposites. *J. Phys. Chem. C* **2008**, *112*, 19841–19845.

(8) Goncalves, G.; Marques, P. A. A. P.; Granadeiro, C.M.; Nogueira, H.I.S.; Singh, M.K.; Grácio, J. Surface Modification of Graphene Nanosheets with Gold Nanoparticles: The Role of Oxygen Moieties at Graphene Surface on Gold Nucleation and Growth. *Chem. Mater.* **2009**, *21*, 4796–4802.

(9)Ferrari, A. C.; Robertson, J. Interpretation of Raman Spectra of Disordered and Amorphous Carbon. *J. Phys. Rev. B* **2000**, *61*, 14095−14107.

(10) Appel, A. M.; Bercaw, J. E.; Bocarsly, A. B.; Dobbek, H.; DuBois, D. L.; Dupuis, M.; Ferry, J. G.; Fujita, E.; Hille, R.; Kenis, P. J. A.; Kerfeld, C. A.; Morris, R. H.; Peden, C. H. F.; Portis, A. R.; Ragsdale, S. W.; Rauchfuss, T. B.; Reek, J. N. H.; Seefeldt, L. C.; Thauer, R. K.; Waldrop, G. L. Frontiers, Opportunities, and Challenges in Biochemical and Chemical Catalysis of CO_2 Fixation. *Chem. Rev.* **2013**, *113*, 6621−6658.